

Dynamics and deposition of sediment-bearing multi-pulsed flows and geological implication

Ho, Viet Luan; Dorrell, Robert M.; Keevil, Gareth; Thomas, Robert E.; Burns, Alan D.; Baas, Jaco H.; McCaffrey, William D.

Journal of Sedimentary Research

Published: 01/11/2019

Peer reviewed version

[Cyswllt i'r cyhoeddiad / Link to publication](#)

Dyfyniad o'r fersiwn a gyhoeddwyd / Citation for published version (APA):

Ho, V. L., Dorrell, R. M., Keevil, G., Thomas, R. E., Burns, A. D., Baas, J. H., & McCaffrey, W. D. (2019). Dynamics and deposition of sediment-bearing multi-pulsed flows and geological implication. *Journal of Sedimentary Research*, 89(11), 1127-1139.

Hawliau Cyffredinol / General rights

Copyright and moral rights for the publications made accessible in the public portal are retained by the authors and/or other copyright owners and it is a condition of accessing publications that users recognise and abide by the legal requirements associated with these rights.

- Users may download and print one copy of any publication from the public portal for the purpose of private study or research.
- You may not further distribute the material or use it for any profit-making activity or commercial gain
- You may freely distribute the URL identifying the publication in the public portal ?

Take down policy

If you believe that this document breaches copyright please contact us providing details, and we will remove access to the work immediately and investigate your claim.

1 DYNAMICS AND DEPOSITION OF SEDIMENT-BEARING MULTI-PULSED FLOWS AND
2 GEOLOGICAL IMPLICATION

3 Viet Luan Ho^{1*}, Robert M. Dorrell², Gareth M. Keevil¹, Robert E. Thomas³, Alan D. Burns⁴,
4 Jaco H. Baas⁵, William D. McCaffrey^{1†}

5 ¹School of Earth and Environment, University of Leeds, Leeds, UK, LS2 9JT, ²Faculty of
6 Science and Engineering, University of Hull, Hull, UK, HU6 7RX, ³Energy and Environment
7 Institute, University of Hull, Hull, UK, HU6 7RX, ⁴School of Process and Chemical Engineering,
8 University of Leeds, Leeds, UK, LS2 9JT, ⁵School of Ocean Sciences, Bangor University,
9 Anglesey, UK, LL59 5AB.

10 *Currently at Imperial College London, London, UK, SW7 2AZ.

11 †Corresponding author: William D. McCaffrey, W.D.McCaffrey@leeds.ac.uk

12 Key words: multi-pulsed turbidites, pulsed turbidites, multi-pulsed flows, single-pulsed
13 turbidites, sediment-bearing flows

14 **ABSTRACT**

15 Previous studies on dilute, multi-pulsed, subaqueous saline flows have demonstrated that
16 pulses will inevitably advect forwards to merge with the flow front. On the assumption that
17 pulse merging occurs in natural-scale turbidity currents, it was suggested that multi-pulsed
18 turbidites that display vertical cycles of coarsening and fining would transition laterally to
19 single-pulsed, normally-graded turbidites beyond the point of pulse merging. In this study,
20 experiments of dilute, single- and multi-pulsed sediment-bearing flows (turbidity currents)
21 are conducted to test the linkages between downstream flow evolution and associated
22 deposit structure. Experimental data confirm that pulse merging occurs in laboratory-scale
23 turbidity currents. However, only a weak correspondence was seen between longitudinal
24 variations in the internal flow dynamics and the vertical structure of deposits; multi-pulsed

deposits were documented, but transitioned to single-pulsed deposits prior to the pulse merging point. This early transition is attributed to rapid sedimentation-related depletion of the coarser-grained suspended fraction in the laboratory setting, whose absence may have prevented the distal development of multi-pulsed deposits; this factor complicates estimation of the transition point in natural-scale turbidite systems.

INTRODUCTION

Turbidity currents are dilute, subaqueous particle-laden gravity currents (Middleton 1993; Piper & Savoye 1993; Huppert 1998; Xu et al. 2004). They commonly initiate on continental shelves and transport significant volumes of sediment from the continents to deep marine environments (Simpson 1982; Talling et al. 2015), where they build the most spatially extensive sedimentary landforms on the planet (Canals et al. 2004; Xu 2011; Dorrell et al. 2015; Lintern et al. 2016).

Turbidity current deposits – turbidites – can be used to infer the dynamics of the overpassing flows (Hand 1997; Goldfinger et al. 2012; Kneller & McCaffrey 2003). Turbidites are formed as turbidity currents decelerate and material is deposited from suspension. Because particle-transport competence (i.e., the maximum particle-size that can be transported) decreases as flow wanes (Dorrell et al. 2013), turbidites commonly exhibit classic upward-fining grading structures. These “single-pulsed” turbidites are thus interpreted to reflect a single depositing turbidity current event (Hand 1997; Kneller & McCaffrey 2003; Amy et al. 2006; Dorrell et al. 2011a; Stevenson et al. 2013). However, “pulsed” or “multi-pulsed” turbidites characterised by repeated cycles of inverse-to-normal grading (with or without grain size breaks) are also seen higher up within a single event-bed in real world environments (Goldfinger et al. 2012; Stevenson et al. 2014; Van Daele et al. 2017). This feature is different from the inverse-graded intervals which characterise many

turbidite bed bases (see Hand 1997). Multi-pulsed turbidites are therefore thought to be deposited by turbidity currents whose longitudinal velocity structures show repeated patterns of waxing-waning mean velocity, and thus variations in flow capacity and competence (Dorrell et al. 2013, 2018; Stevenson et al. 2014). Such currents can be initiated by: i) retrogressive submarine slumping occurring due to sequential earthquake faulting or shock/aftershock events; ii) combination of multiple single-pulsed flows sourced in different upstream areas at downstream confluences (Goldfinger et al. 2012; Ismail et al. 2016; Beeson et al. 2017; Johnson et al. 2017); and iii) variation in discharge rates of sediment fluxes from fluvial systems into the oceans (Mulder & Alexander 2001).

Experimental data describing the dynamics of multi-pulsed saline gravity currents, presented in Ho et al. (2018a) and Ho et al. (2018b), suggest that initially multi-pulsed velocity structures transform into standard waxing-waning profiles as flows run out. The principal implication was that any associated turbidites would likely exhibit multi-pulsed grading profiles relatively proximally to the source, but that the deposits would become normally graded past the point where pulses within the flows merge completely. A second implication was that, approaching this point, the spatial separation between multiple cycles of inverse-to-normal grading within a single turbidite would progressively reduce, reflecting the progressive reduction in the temporal separation between multiple velocity pulses. These implications are based on the assumptions that: a) normally graded turbidite intervals are deposited in the waning phase of flows and non-deposition or the deposition of upward-coarsening turbidite intervals is expected during the waxing phase (Kneller & Branney 1995; Hand 1997; Kneller & McCaffrey 2003; Amy et al. 2005; Basilici et al. 2012); b) flows are depositional from the outset, with flow conditions being recorded in the deposit during progressive aggradation (Basilici et al. 2012; Goldfinger et al. 2013); c) a wide enough range

of grain sizes is carried in suspension for a link between the flow shear stress and grain size to be expressed in the deposit (Dorrell et al. 2013); and d) that there is sufficient time for the suspension to respond to changes in flow conditions (Dorrell & Hogg 2011b).

Questions regarding the variation of flow dynamics in sediment-bearing multi-pulsed flows and their expression in depositional structures along flow pathways include: i) whether the merging phenomenon observed in the saline flow experiments can be reproduced for multi-pulsed turbidity currents; ii) whether any grading patterns within deposits can be discerned; and iii) whether linkages can be established between real-time suspension structures of sediment within the flows and depositional grading patterns. To address these questions, this paper details the first experiments conducted to model multi-pulsed sediment-bearing flows, focusing on the difference in dynamics between single- and multi-pulsed turbidity currents linked to the vertical grading profiles of their deposits.

METHODOLOGY

Experimental Set-up and Parameters

Experiments were conducted in a 5 m-long flume with two 0.25 m-long lockboxes set-up at one end (Fig. 1). This set up of the lockboxes enabled the generation of two pulses in series. Both single- and multi-pulsed flows entailed release of flow pulse components of the same volume. Using electronically-timed pneumatic rams, the timing between the two lock gate release was set at 0 s, 2.5 s and 8 s in order to model two flow types, i.e., single- and multi-pulsed flows. It should be noted that by 2.5 s after the first lock gate was withdrawn, the returning wave generated by the collapse of the first dense fluid had not reached the back of the first lockbox such that the dynamical variations between the 0 s and 2.5 s delay time flows were expected to be minimal (see section 3.1 and Ho et al. 2018b for discussion). Therefore, both 0 s and 2.5 s delay time flows were effectively single-pulsed flows, whereas

an 8 s delay time enabled the generation of multi-pulsed flows. The dense fluid used for the flows was made of a mixture of fresh water and 625 g of suspended sediment consisting of both spherical Ballotini and Spherglass in the ratio 4:1 by weight; sediment size ranged between 5 and 120 μm (see Appendix A). The density of sediments was 2500 kgm^{-3} (Potters 2018). This combination of sediments gave the suspension an initial excess density of 3.75%, corresponding to a volumetric concentration of 2.5%. Sediments in the lockboxes were kept in suspension by using two MESE^R overhead stirrers that were set to run at 1000 rpm at the start of the experiments. Each mixer was fitted with a switch that automatically stopped it as the gate in front was lifted (Fig. 1). The depth of fluid contained in the two lockboxes and of freshwater in the flume was 0.20 m. The flow component in the second lock was dyed blue in order to enhance the visualisation of the flows. In order to confirm that pulses within the multi-pulsed flows eventually merged, the front positions of two pulses were tracked separately using two moving cameras which were set on a track in front of the flume (method after Ho et al. 2018b).

Experimental Approach and Data Processing

Profiling Acoustic Doppler Velocimetry

Two acoustic Doppler velocity profilers (Nortek Vectrino Profilers; aDvps) were deployed to measure time-series velocity fields at positions 1.7 m, 2.7 m and 3.7 m along the flume (see Fig. 1). The probes were mounted vertically on two rods spaced 0.1 m apart in the streamwise direction, the two probes were synchronised using Nortek's MIDAS data acquisition software (Nortek 2015) and set to collect velocity profiles at 100 Hz until the flow ceased. The upstream transducer was mounted 81 mm above the channel floor (i.e., bottom of the tank) and recorded the velocity profile in 21, 1 mm-high, cells between 19.5 mm and 40.5 mm above the bottom of the tank. The downstream transducer was mounted

61 mm above the channel floor and recorded the velocity profile in 21, 1 mm-high, cells between 0 mm and 20.5 mm above the floor (see Fig. 1). The vertical overlap between the sampling regions of the two probes was 1 mm. Prior to lock release, the ambient fluid in front of the aDvp probes was seeded with neutrally-buoyant hollow glass spheres of 10 μm diameter (Spherical 110-P8) to raise the Signal-to-Noise Ratio to at least 25 dB (see Thomas et al. 2017). Two sets of aDvp data were collected in each experiment, measuring the velocity field of the upper and lower halves of the basal 40 mm of flow. These data sets were merged to visualise the velocity field within the whole flow. Streamwise velocity data were plotted as a series of isovel maps that displayed spatio-temporal variations of velocity within the basal 40 mm of flow for each current. Depth-averaged velocities were also calculated for both data sets (method after Ho et al. 2018a, averaging over 20 mm). The lateral offset of 0.10 m between the two aDvp probes (see inset, Fig. 1) resulted in a temporal displacement in the two data sets collected, such that within the first ~ 2 seconds of any sampling period only velocities within the top half of the basal 40 mm of flow were captured. This is because the flows always arrived at the upper aDvp probe first.

Focused Beam Reflectance Measurement (FBRM)

In order to quantify the particle size distributions (PSD) within the experimental flows, a Focused Beam Reflectance Measurement system (FBRM) was deployed. FBRM uses a rotating laser beam to measure the chord length distribution (CLD) of all the particles present within the measurement window every two seconds over a defined time period (e.g., Wynn 2003; Greaves et al. 2008; Agimelen et al. 2015). The CLD were then converted to PSD using the conversion method of Wynn (2003), which assumes that all the sediment particles are spherical. The FBRM was deployed so that the centre of the measurement window was located 20 mm above the channel floor, the approximate height of the velocity

maximum as noted in earlier experiments. FBRM data were acquired at 1.85 m, 2.85 m and 3.85 m along the flume (Fig. 1). The FBRM probe was deployed at an inclination of 45°, pointing upstream in order to effectively capture the arrival of suspended particles (see inset, Fig. 1). This configuration minimised the stagnation zone between the measurement window and the flow (set up recommended by the manufacturer, Mettler-Toledo 2013). The cross-sectional area of the 30 mm diameter FBRM probe was relatively small such that it did not interfere with the evolution of the flows at the point of measurement. In addition, no measurements were taken downstream of positions where the FBRM probe was set up.

Sediment data

Deposits were sampled and analysed for the 2.5 s and 8 s delay time flow experiments in order to compare their depositional structures; as noted above the 2.5 s delay time deposits effectively represent a single-pulsed turbidite. Deposits were collected at positions 0.7 m, 1.7 m, 2.7 m, 3.7 m and 4.7 m downstream. Five pieces of 0.25 mm-thick acetate sheet of dimensions 0.12 m by 0.12 m were glued on the bottom of the flume at the positions where deposits were to be sampled; sediment was deposited on top of these sheets. Once the sediments had completely settled (after two days), ambient water was slowly discharged from the flume by siphoning. Plastic rings of 0.10 m diameter were placed onto the acetate in order to secure the deposits. The sediment samples were further allowed to fully dry at room temperature over two days before careful removal from the flume. Each dry sample was impregnated with low-viscosity two-part adhesive under partial vacuum and mounted into transparent cubes. The surface of the mounted samples was polished, and carbon coated to enable imaging using a Tescan VEGA3 Scanning Electron Microscope (SEM). Grading trends were sufficiently subtle to not be immediately evident from visual inspection, necessitating an image analysis approach. Therefore, the SEM images were

processed using MatLab™ 2016, using code based on the Granulometry of Snowflakes example (Mathworks 2018) to calculate grain size. In brief, on each image this entailed performing morphological opening operations using circular structuring elements of progressively increasing size and then differentiating the resulting pixel counts to yield the number of pixels associated with each size circle. Finally, the results were scaled and classified into $\frac{1}{4}\phi$ classes.

RESULTS

Visualisation

The single-pulsed (0 s and 2.5 s delay time; Figs. 2 and 3) and multi-pulsed (8s delay time; Fig. 4) flows evolved in a similar manner to single- and multi-pulsed saline flows (see Ho et al. 2018a and Ho et al. 2018b for details of the flow visualisation approach). Hereafter, both 0 s and 2.5 s delay time flows are referred to as single-pulsed flow and 8 s delay time flow is referred to as multi-pulsed flow.

Velocity Data

Single-pulsed Flow (0 s and 2.5 s delay time)

The velocity profiles of these flows exhibited a normal waxing-waning velocity structure as commonly observed in laboratory and field-based data (Figs. 5A-B & 6A-B; e.g., Simpson 1982; Kneller et al. 1999; Lowe et al. 2002; Cooper et al. 2013; Sher & Woods 2015; Ho et al. 2018a, 2018b). The velocity maximum was located within the bottom 40 mm of the flow (Figs. 5) with body velocities higher than those of the flow fronts. The flows decelerated downstream (Figs. 5A-B). The thicknesses of the heads were also seen to decrease with increasing time.

Multi-pulsed Flow (8 s delay time)

Proximal to the source, two distinct pulses were seen in the velocity structure of the flow (Figs. 5C and 6C, $x=1.7$ m). The second pulse travelled at higher velocity than that of the first pulse (Figs. 5C, $x=1.7$ m). Further downstream, the first pulse decelerated while the second pulse maintained a relatively high velocity which enabled it to catch up with the first pulse (Figs. 5C and 6C, $x=2.7$ m). The separation between the two pulses was progressively reduced over time such that the pulses eventually merged (Figs. 5C and 6C). Flow visualisation data captured during the experiments suggest that pulses within the 8 s delay time flow merged at 4.05 m from source (i.e., at the position $x=4.20$ m shown on the gridline, Figs. 1 and 4). However, due to space constraints at the end of the flume, aDvp data could not be collected beyond 4.0 m.

Sediment Suspension Profiles

In this section, profiles of sediment suspension at 20 mm flow height are described for the single-pulsed (0 s and 2.5 s) and the multi-pulsed (8 s) flows, respectively. The time-series patterns of sediment suspension at this characteristic height, measured at different downstream positions, are thought to be indicative of the temporal variations of sediment suspension at any given height within the flows. PSDs were bimodal in form at every time step, though the range of size classes varied in each data set (Fig. 7) as will be described below.

At proximal localities, the number of particles arriving at the sampling position progressively decreased as the heads passed by the probe (Figs. 4A-C, $x=1.85$ m). Particle counts were relatively stable within the bodies of the flows (Figs. 4A-C, $x=2.85$ m & $x=3.85$ m).

Single-pulsed Flow

Mean grain size gradually increased as the flow head passed by the sampling position. Initially, sediments of 20-60 μm had been carried by the flow front over the first 5 s of the sampling period, prior to the arrival of the body (Figs. 7A-B, $x=1.87\text{ m}$, 15-20 s). After the passage of the heads, mean grain size (i.e., sizes of sediment ranged within 30-90 μm) started to increase, which marked the arrival and passage of the flow bodies. At further distances, fine-grained sediments of 20-60 μm were always suspended in the flow fronts (Figs. 4A-B, $x=1.85\text{ m}$, 13-20 s; $x=2.85\text{ m}$, 25-30 s; $x=3.85\text{ m}$, 32-36 s) whereas coarser sediments of 30-90 μm were carried by the body and the tail (Figs. 4A-B, $x=1.85\text{ m}$, 40 s; $x=2.85\text{ m}$, 40 s).

Multi-pulsed Flow

Sediments of 20-60 μm grain size were suspended in the flow front within the first 5 s after the flow passed the probe; grain sizes then increased to range within 30-90 μm as the flow head moved past the sampling position (Fig. 7C, $x=1.85\text{ m}$, 15-20 s). The arrival of a second pulse was marked by a decrease in grain size (Fig. 7C, $x=1.85\text{ m}$, $t=18\text{ s}$). After the second pulse front passed the probe, sediment grain size started to increase (Fig. 7C, $x=1.85\text{ m}$, $t=21\text{ s}$). Similarly, at $x=2.85\text{ m}$, the suspended sediment grain size within the flow front increased as the first pulse arrived but decreased as a second pulse started to intrude into the first pulse (Fig. 7C, $x=2.85\text{ m}$, 33-40s). Further downstream, at the position where the two pulses were close to merging, the range of grain size remained relatively constant (Fig. 7C, $x=3.85\text{ m}$).

Sediment Data

In this section, data describing depositional structures of single-pulsed (2.5 s delay time) and multi-pulsed (8 s delay time) flows are presented in the order of i) trends observed for all deposits and ii) different features in depositional profiles of each flow type.

The experimental data showed that thicknesses of the deposits collected in the experiments decreased as the flows travelled further from the source (Fig. 8). This observation corroborates previous studies (e.g., Kneller & Branney 1995; Mulder & Alexander 2001; Harris et al. 2002; Shanmugam 2002). For each experiment (i.e., each flow type), data detailing the vertical variations in grainsize of fine, median and coarse sediment fractions (i.e., d16, d50 and d84) showed similar trends (Fig. 8, d16, d50 and d84 for each flow type at five sampling positions). Basal inverse-graded deposition was observed for the deposits of both flow types (Fig. 8) and was attributed to longitudinal grain size segregation (Hand 1997; Baas et al. 2004). Above the inverse-graded interval, normal grading was generally developed, with an abrupt reduction in the fining-up gradient occurring at about two-thirds deposit height.

Single-pulsed Flow

All deposits collected in the single-pulsed flow experiment exhibited upward-fining grading profiles after the basal inversely-graded interval (Fig. 8, data indicated by blue line; cf., Kneller & McCaffrey 2003; Amy et al. 2005; Babonneau et al. 2010 for similar observations). The proximal deposit (0.7 – 1.7 m) was thicker than the deposit downstream (3.7 - 4.7 m) by approximately 50%. This observation of thicker deposits near the lock gates is commonly seen in lock-exchange sediment-bearing flow experiments and models (Fig. 8; Bonnetaze et al. 1993; Kneller & McCaffrey 2000; Peakall et al. 2001; Harris et al. 2002).

Multi-pulsed Flow

The thickness of the deposits sampled proximal to the source, at 0.7 m, 1.7 m and 2.7 m, was greater than that of deposits taken at distal locations by 50%. At 1.7 m, the flow deposited proximal turbidites with a higher fraction of coarse sediments (Fig. 8C, 0.7 m). Vertical grading of the coarse fraction deposited by this flow showed two intervals of

inverse-to-normal grading (Fig. 8C, 0.7 m, red curve). It was noted that the pulses in the flow this experiment merged at 4.2 m down the flume, but the flow deposited sediments with simple upward-fining grading structures from at least 1.7 m (Fig. 8C).

DISCUSSION

The Initiation and Dynamics of Single- and Multi-pulsed Flows

To predict whether multi-pulsed flows will be generated, the timing interval between pulses at initiation (i.e., between the release of successive lock gates, or between two currents in natural settings) needs to be constrained. In the laboratory setting, the minimum value for which a multi-pulsed flow is formed corresponds to the time taken for the backwards-propagating wave generated upon the slumping of the first pulse to reach the second lock gate, corresponding a distance of one lock length. If the wave has not reached this gate before it is raised, the combined flow is the same as the instantaneous release of a double-length lock (i.e., Figs. 5 and 6 show the dynamical similarity of the 0 s and 2.5 s flows; see also Ho et al. 2018b). In prototype environments, delay time between pulses may range from minutes to hours, or longer, depending on the nature of the initiation mechanism (e.g., Hsu et al. 2008; Goldfinger et al. 2012; Lupi & Miller 2014; Beeson et al. 2017). In the real-world, single-pulsed flows are generated either by a single-trigger event, or by two (or more) events whose temporal separation is insufficient to form separate flow events.

Experimental data demonstrate that material from the body of both single- and multi-pulsed flows is eventually advected toward the flow fronts (Figs. 2-4). Advection of fluid within the body of dilute gravity currents towards the flow front is ubiquitous due to their internal velocity profiles (Lowe et al. 2012; Stevenson et al. 2013; Sher & Woods 2015; Hughes 2016). Therefore, single- and multi-pulsed flows cannot be distinguished by

advection of material from back to front of the flow. The key criterion is the development of one or more episodes of increasing then decreasing mean velocity in the multi-pulsed case compared to the monotonic decrease in mean velocity seen in the single-pulse case (e.g., Figs. 5, 6).

Single-pulsed Flow Deposits

Deposits derived from single-pulsed flows are thicker closer to source than downstream, e.g. deposits at 0.7-2.7 m were 50% thicker than those at 3.7-4.7 m (Fig. 8). In addition, a high proportion of coarse-grained sediments are deposited proximally (Fig. 8; see also Middleton 1993; Gladstone et al. 1998; Kneller & McCaffrey 2003). In general, as suggested by the experimental data (Fig. 8), single-pulsed flows deposit sediments with the expected upward-fining grain size profile (e.g., Bouma 1962; Lowe 1982). Inverse grading in the basal part of deposits is also seen (e.g., Fig. 8), probably reflecting the lagged arrivals at the head of sediments with different grain size (e.g., Kneller & Branney 1995; Hand 1997). Sediment suspension data from single-pulsed flows (Figs. 7A-B) indicate that relatively finer sediments (20-60 μm) are carried by flow fronts, whereas coarser sediments (30-90 μm) are suspended within the bodies. Although translation of these longitudinal variations in mean grain size into grading profiles is apparently consistent with the lagged-arrival model of Hand (1997), the FBRM data in this study were acquired 20 mm from the base of the flow, i.e., above the depositional interface; it is likely that sediments carried below this level would have been coarser grained due to the stratification commonly developed within turbidity currents (e.g., McCaffrey et al. 2003; Baas et al. 2005; Dorrell et al. 2014; Ho et al. 2018a). Nevertheless, on the assumption that relative temporal variations in grain size composition at any particular level are likely representative of variations seen at lower levels, the lagged arrival mechanism remains a viable explanation of basal inverse-graded interval formation. It is

difficult to invoke other causes of inverse grading, such as a marked interval of waxing flow (Kneller and McCaffrey 2003; Stevenson et al. 2014) or kinetic sieving within the basal flow layer under low deposition rates (cf. Sumner et al. 2008) as the single-pulse experiments entailed relatively rapid deposition under waning flow.

Multi-pulsed Flow Deposition

Based on the interpretation of saline multi-pulsed flow experiments, Ho et al. (2018a, 2018b) suggested that multi-pulsed turbidites would persist up to the point of merging, with normally-graded turbidites deposited thereafter. However, the data collected in this study show only weak proximal development of multi-pulsed grading, expressed as two intervals of inverse-to-normal grading in the d84 grainsize fraction at the most proximal measured position (red trace in Fig. 8C, at 0.7m); otherwise normal grading patterns develop well before the merging point (see section 3.4, above). The links between the longitudinal variation of flow velocity structure, the grainsize of sediments falling from suspension in any particular location and the resultant deposit grading profiles are unclear. An explanation is therefore developed to account for the observed patterns of deposition; it assumes that sediments aggrade progressively from overpassing flows (e.g., Choux & Druitt 2002; Kneller & McCaffrey 2003; Amy et al. 2005).

Prior to the second release, it is thought that the first pulse developed vertical density stratification due to incipient deposition and entrainment of ambient fluid. Ambient water entrainment occurs both at the flow front and above the flow body (Hallworth et al. 1993; Sher & Woods 2015; Dorrell et al. 2016). Density stratification is also enhanced by particle sedimentation (Middleton & Hampton 1973; van de Berg et al. 2017). Therefore, a relatively-concentrated near-bed layer with a high proportion of faster-settling coarse sediments may develop, with more dilute flow above due to ambient water entrainment

(e.g., Kneller & Buckee 2000; see also Stevenson 2014); the point of transition may not correspond to the level of the velocity maximum. In the absence of near-bed flow data, it cannot be determined if the basal layer became sufficiently dense such that grain-grain interactions affected sediment deposition (e.g., Stevenson et al. 2014).

At proximal locations, the deposition of multi-pulsed turbidites is reflective of the longitudinal variation in mean grain size of the overpassing flow immediately above the depositional interface. Sediments comprising the near-bed layer of the first pulse are deposited. At the depositional interface, slightly finer sediments are likely carried by the pulse front and slightly coarser sediments by the body and the tail (e.g., Hand 1997, McCaffrey et al. 2003; Baas et al. 2005; Fig. 7). Assuming that the response time-scale of sediments in suspension is near-instantaneous (Dorrell & Hogg 2011), the vertical structure of deposits attributed to the first pulse at any location would exhibit the classic inverse graded base succeeded by an upward-fining profile. The head of the second pulse is associated with a local increase in mean flow velocity (i.e., waxing flow; Figs. 5, 6). Coarse material transported in the second pulse thus interacts with the relatively finer particles composing the tail of the first flow (Dorrell et al. 2011, 2013). Coarser sediments within this second pulse falling from suspension, either directly onto the bed, or through a vestigial basal layer associated with the first pulse, will result in an upward-coarsening trend principally expressed through variations within the coarsest sediments (e.g., via a measure such as d_{84}). Such deposition is followed by that of the fine sediment remnants of both pulses. The proximal compound deposit will therefore show a multi-pulsed vertical grading pattern (e.g., Fig. 8C, 0.7 m). The inverse graded intervals within a multi-pulsed turbidite may arise either due to longitudinal coarsening within the second pulse, or due to the grainsize difference between finer-grained sediments attributed to the first pulse and

coarser sediments attributed to the second or due to a combined effect; the data do not readily allow these possibilities to be discriminated.

Because the second pulse travels more quickly than the flow head (Ho et al. 2018a), the time-period between its arrival and that of the head progressively reduces down the flume; in addition this pulse is thought to rapidly deplete in coarser sediments due to proximal deposition. Therefore both the difference in the grain size of suspended sediments between successive pulses and the time for the depositional boundary to react to changing flow conditions (see Dorrell & Hogg 2011) progressively reduce distally; jointly these effects are thought to suppress any multi-pulsed signature in the deposit grading pattern. The spatial scales over which coarse sediments in the second pulse are carried within the basal layer cannot be deduced directly in this study, preventing estimation of the spatial persistence of multi-pulsed turbidite deposition caused by flow surging. Consequently, if it is applicable to turbidity currents, the scaling analysis conducted by Ho et al. (2018b) based on data from saline flows only provides an upper limit on merging lengths; single-pulsed turbidites may form before this point.

Methodological and Modelling Limitations

The development of single-pulsed turbidites prior to point of merging may result from the experimental modelling approach. The proportion of coarse sediments in the initial pulses of dense fluid was smaller than those of finer sediment classes (see Appendix A). Since the inverse-to-normal grading of multi-pulsed turbidites appears to be expressed principally in the relative distributions of coarser grained sediments (e.g., Fig. 8C, 0.7 m), the small proportion of such sediments might contribute to the absence of discernible multi-pulsed turbidites before the merging point. A contrary explanation is that the limit of coarse sediment transport (and thus the development potential of multi-pulsed turbidites prior to

the point of merging) may depend upon the presence of finer grained particles. This is because increasing the relative proportion of finer grain sizes is known to increase the distance of coarse sediment transport; finer sediments remain in suspension over longer times and thus sustain the associated flows (Gladstone et al. 1998, Gladstone & Woods 2000; Harris et al. 2002).

The focus of this contribution has been on the development of cycles of inverse to normal grading within turbidites (e.g., Sumner et al. 2008; Ho et al. 2018a, 2018b). However, this topic can be placed within a broader evaluation of the development of variable grading patterns and their causes including the development of basal inverse grading (e.g., Hand, 1997; Sumner et al. 2008) and of grain size breaks (Kneller and McCaffrey 2003; Stevenson et al. 2014). Thus, patterns of repeated coarsening and fining produced in annular flume experiments have been related to episodes of erosion and deposition within slowly aggrading deposits associated with development of sedimentary laminae (Sumner et al., 2008); as noted above, the inverse grading documented in the experiments reported here is unlikely to have formed by this process. Stevenson et al. (2014) document a range of examples of abrupt grain size breaks within turbidites sampled along deposition transects > 2000 km length in the Moroccan Turbidite System. Those related to deposition beneath Newtonian flows are explained by flows waxing to bypass or bypassing due to changes between capacity- vs. competence related deposition to explain the superposition of finer-grained over coarser-grained sediments (see also McCaffrey and Kneller, 2003; Kane et al. 2009). However, flow waxing alone is invoked to explain those cases in which inverse grading is seen within the coarser-grained intervals. Erosion and bypassing may occur in prototype environments during significant periods of a flow (e.g., Rimoldi et al. 1996; Sultan et al. 2007; Stevenson et al. 2013; 2014); as well as causing grain size breaks in their own

right such processes may also affect the development of surge-related multi-pulsed turbidites, which may be distorted and/or destroyed due to non-deposition or erosion. This subject remains a topic for future study.

CONCLUSIONS

Experiments conducted to study the dynamics of single- and multi-pulsed turbidity currents confirm that after an initial period of abruptly waxing velocity, the mean velocity of single-pulsed currents reduces monotonically in the waning phase, whereas that of multi-pulsed flows transitions from waxing-waning cycles to monotonic reduction in their waning phase. This pattern is similar to that observed in the dynamics of multi-pulsed saline flows (Ho et al. 2018a) and confirms that intra-flow velocity pulses are advected forwards, eventually reaching the flow front at pulse merging points. The work further confirms that a minimum threshold separation time between the release of individual pulses is required if the resulting flows are to exhibit multi-pulsed character. In the experimental scenario, this minimum delay period corresponds to the time required for the backward-propagating wave generated upon the collapse of the first pulse to reach the second lock gate. Pulse delay periods less than the threshold interval result in the development of single-pulsed flows.

Although the data support the inference of Ho et al. (2018a and b) that initiation signals may potentially be expressed through the development of multi-pulsed turbidites and that normally graded turbidites found beyond the final point of pulse merging cannot express such signals, the assumed correspondence between the merging point and the cessation of multi-pulsed turbidite deposition was not confirmed; the transition occurred well upstream. Therefore, if the scaling analysis derived for saline flows (e.g., Ho et al. 2018b) is used to predict pulse merging points in natural scale turbidity currents, it can

provide only an upper limit to the distance over which multi-pulsed turbidites may be developed. Whether or not multi-pulsed turbidites persist up to the merging point depends upon the transport potential of coarser grains carried within pulses; the optimal grain size distribution to maximise this potential remains unknown.

Acknowledgements

This work was funded by Turbidites Research Group (TRG, Sponsors: Anadarko, BP, ConocoPhillips, Dana Petroleum, ENI, HESS, Nexen, OMV, Petronas, Shell, Statoil, Tullow, Woodside). None of the authors have any conflict of interest to declare. We would like to thank i) Helena Brown in the Sorby Environmental Fluid Dynamics Laboratory for her assistance with the experiments; ii) Harri (John Wynn) Williams in the thin section laboratory for helping with producing sediment samples; and iii) Richard Walshaw, Duncan Hedges in the Electron Microscopy and Spectroscopy Centre for their support with using the SEM. This manuscript was developed upon part of Ho's (2018) PhD thesis, deposited on the White Rose Research Online repository. Data describing the composition, i.e., size and shape, of sediments used in the lockboxes are shown in the supplementary material. We would also like to thank the Associate Editor and two reviewers whose comments on the previous version of this manuscript have helped improve the paper.

References

Agimelen, O.S., Hamilton, P., Haley, I., Nordon, A., Vasile, M., Sefcik, J. and Mulholland, J., 2015, Estimation of particle size distribution and aspect ratio of non-spherical particles from chord length distribution, *Chemical Engineering Science*, v. 123, p. 629-640.

453 Amy, L.A., Peakall, J. and Talling, P.J., 2005, Density- and viscosity-stratified gravity currents:
 454 Insight from laboratory experiments and implications for submarine flow deposits,
 455 Sedimentary Geology, v. 179, p. 5-29.

456 Baas, J.H., McCaffrey, W.D., Haughton, P.D.W. and Choux, C.M.A., 2005, Coupling between
 457 suspended sediment distribution and turbulence structure in a laboratory turbidity
 458 current, Journal of Geophysical Research-Oceans, v. 110, C11015.

459 Baas, J.H., van Kesteren, W. and Postma, G., 2004, Deposits of depletive high- density
 460 turbidity currents: a flume analogue of bed geometry, structure and texture,
 461 Sedimentology, v. 51, p. 1053-1088.

462 Babonneau, N., Savoye, B, Cremer, M. and Bez, M., 2010, Sedimentary architecture in
 463 meanders of a submarine channel: Detailed study of the present Congo turbidite
 464 channel (Zaiango project), Journal of Sedimentary Research, v. 80, p. 852- 866.

465 Basilici, G., de Luca, P.H.V. and Poiré, D.G., 2012, Hummocky cross-stratification- like
 466 structures and combined-flow ripples in the Punta Negra Formation (Lower-Middle
 467 Devonian, Argentine Precordillera): A turbiditic deep-water or storm-dominated
 468 prodelta inner-shelf system? Sedimentary Geology, v. 267-268, p. 73-92.

469 Beeson, J.W., Johnson, S.Y., Goldfinger, C. and Ross, A.F., 2017, The transtensional offshore
 470 portion of the northern San Andreas fault: Fault zone geometry, late Pleistocene to
 471 Holocene sediment deposition, shallow deformation patterns, and asymmetric basin
 472 growth, Geosphere, v. 13, p. 1-34.

473 Bonnecaze, R.T., Huppert, H.E. and Lister, J.R., 1993, Particle-driven gravity currents, Journal
 474 of Fluid Mechanics, v. 250, p. 339-369.

475 Bouma, A.H., 1962, Sedimentology of some Flysch Deposits: A Graphic Approach to Facies
 476 Interpretation, Elsevier, Amsterdam, p. 168.

477 Canals, M., Lastras, G., Urgeles, R., Casamor, J.L., Mienert, J., Cattaneo, A., De Batist, M.,
478 Haflidason, H., Imbo, Y., Laberg, J.S., Locat, J., Long, D., Longva, O., Masson, D.G.,
479 Sultan, N., Trincardi, F. and Bryn, P., 2004, Slope failure dynamics and impacts from
480 seafloor and shallow sub-seafloor geophysical data: Case studies from the COSTA
481 project, *Marine Geology*, v. 213, p. 9-72.

482 Choux, C.M. and Druitt, T.H., 2002, Analogue study of particle segregation in pyroclastic
483 density currents, with implications for the emplacement mechanisms of large
484 ignimbrites, *Sedimentology*, v. 49, p. 907-928.

485 Dorrell, R. M. and Hogg, A. J., 2011b, Length and time scales of response of sediment
486 suspensions to changing flow conditions, *Journal of Hydraulic Engineering*, v. 138, p.
487 430-439.

488 Dorrell, R. M., Burns, A. D. and McCaffrey, W. D., 2015, The inherent instability of leveed
489 seafloor channels, *Geophysical Research Letters*, v. 42, p. 4023-4031.

490 Dorrell, R. M., Darby, S. E., Peakall, J., Sumner, E. J., Parsons, D. R., & Wynn, R. B., 2014, The
491 critical role of stratification in submarine channels: Implications for channelization
492 and long runout of flows, *Journal of Geophysical Research: Oceans*, v. 119, p. 2620-
493 2641.

494 Dorrell, R. M., Hogg, A. J. and Pritchard, D., 2013, Polydisperse suspensions: Erosion,
495 deposition, and flow capacity, *Journal of Geophysical Research: Earth Surface*, v. 118,
496 p. 1939-1955.

497 Dorrell, R. M., Hogg, A. J., Sumner, E. J. and Talling, P. J., 2011a, The structure of the deposit
498 produced by sedimentation of polydisperse suspensions, *Journal of Geophysical*
499 *Research: Earth Surface*, v. 116, F01024.

500 Dorrell, R.M., Amy, L.A., Peakall, J. and McCaffrey, W.D., 2018, Particle size distribution
 501 controls the threshold between net sediment erosion and deposition in suspended
 502 load dominated flows, *Geophysical Research Letters*, v. 45, p. 1443-1452.

503 Dorrell, R.M., Hogg, A.J. and Pritchard, D., 2013, Polydisperse suspensions: Erosion,
 504 deposition, and flow capacity, *Journal of Geophysical Research: Earth Surface*, v. 118,
 505 p. 1939-1955.

506 Dorrell, R.M., Peakall, J., Sumner, E.J., Parsons, D.R., Darby, S.E., Wynn, R.B., Özsoy, E. and
 507 Tezcan, D., 2016, Flow dynamics and mixing processes in hydraulic jump arrays:
 508 Implications for channel-lobe transition zones, *Marine Geology*, v. 381, p. 181-193.

509 Gladstone, C. and Woods, A.W., 2000, On the application of box models to particle-driven
 510 gravity currents, *Journal of Fluid Mechanics*, v. 416, p. 187-195.

511 Gladstone, C., Phillips, J.C. and Sparks, R.S.J., 1998, Experiments on bidisperse, constant-
 512 volume gravity currents: propagation and sediment deposition, *Sedimentology*, v.
 513 45, p. 833-843.

514 Goldfinger, C., Morey, A.E., Black, B., Beeson, J., Nelson, C.H. and Patton, J., 2013, Spatially
 515 limited mud turbidites on the Cascadia margin: segmented earthquake ruptures?
 516 *Natural hazards and earth system sciences*, v. 13, p. 2109-2146.

517 Goldfinger, C., Nelson, C.H., Morey, A.E., Johnson, J.E., Patton, J., Karabanov, E., Gutiérrez-
 518 Pastor, J., Eriksson, A.T., Gràcia, E., Dunhill, G., Enkin, R.J., Dallimore, A. and Vallier,
 519 T., 2012, Turbidite event history—methods and implications for Holocene
 520 paleoseismicity of the Cascadia subduction zone, *U.S. Geological Survey Professional*
 521 *Paper 1661-F*, p. 170. (Available free at <http://pubs.usgs.gov/pp/pp1661f/>).

522 Greaves, D., Boxall, J., Mulligan, J., Montesi, A., Creek, J., Sloan, E.D. and Koh, C.A., 2008,
523 Measuring the particle size of a known distribution using the focus beam reflectance
524 measurement technique, *Chemical Engineering Science*, v. 63, p. 5410-5419.

525 Hallworth, M.A., Phillips, J.C., Huppert, H.E. and Sparks, R.S.J., 1993, Entrainment in
526 turbulent gravity currents, *Nature*, 3v. 62, p. 829-831.

527 Hand, B.M., 1997, Inverse grading resulting from coarse-sediment transport lag, *Journal of*
528 *Sedimentary Research*, v. 67, p. 124-129.

529 Harris, T.C., Hogg, A.J. and Huppert, H.E., 2002, Polydisperse particle-driven gravity currents,
530 *Journal of Fluid Mechanics*, v. 472, p. 333-371.

531 Ho, V.L., Dorrell, R.M., Keevil, G.M., Burns, A.D. and McCaffrey, W.D., 2018a, Pulse
532 propagation in turbidity currents, *Sedimentology*, v. 65, p. 620-637.

533 Ho, V.L., Dorrell, R.M., Keevil, G.M., Burns, A.D. and McCaffrey, W.D., 2018b, Scaling analysis
534 of multi-pulsed turbidity current evolution with application to turbidite
535 interpretation, *Journal of Geophysical Research: Oceans*, v. 123, p.3668-3684.

536 Hsu, S., Kuo, J., Lo, C., Tsai, C., Doo, W., Ku, C. and Sibuet, J., 2008, Turbidity currents,
537 submarine landslides and the 2006 Pingtung earthquake off SW Taiwan, *Terrestrial,*
538 *Atmospheric and Oceanic Sciences*, v. 19, p. 767-772.

539 Hughes, G.O., 2016, Inside the head and tail of turbulent gravity current, *Journal of Fluid*
540 *Mechanics*, v. 790, p. 1-4.

541 Huppert, H.E., 1998, Quantitative modelling of granular suspension flows, *Philosophical*
542 *Transactions of the Royal Society A: Mathematical, Physical and Engineering*
543 *Sciences*, v. 356, p. 2471-2496.

544 Ismail, H., Viparelli, E. and Imran, J., 2016, Confluence of density currents over an erodible
545 bed, *Journal of Geophysical Research*, v. 121, p. 1251-1272.

546 Johnson, H.P., Gomberg, J.S., Hautala, S.L. and Salmi, M.S., 2017, Sediment gravity flows
 547 triggered by remotely generated earthquake waves, *Journal of Geophysical*
 548 *Research: Solid Earth*, v. 122, doi:10.1002/2016JB013689.

549 Kane, I. A., McCaffrey, W. D. and Martinsen, O. J., 2009, Autogenic vs. Allogenic controls on
 550 Megaflute Formation. *Journal of Sedimentary Research* 79(9-10): 643-651.

551 Kneller, B. and Buckee, C., 2000, The structure and fluid mechanics of turbidity currents: a
 552 review of some recent studies and their geological implications, *Sedimentology*, v.
 553 47, p. 62-94.

554 Kneller, B. and McCaffrey, W.D., 2003, The interpretation of vertical sequences in turbidite
 555 beds: the influence of longitudinal flow, *Journal of Sedimentary Research*, v. 73, p.
 556 706- 713.

557 Kneller, B.C. and Branney, M.J., 1995, Sustained High-Density Turbidity Currents and the
 558 Deposition of Thick Massive Sands, *Sedimentology*, v. 42, p. 607-616.

559 Kneller, B.C., Bennett, S.J. and McCaffrey, W.D., 1999, Velocity structure, turbulence and
 560 fluid stresses in experimental gravity currents, *Journal of Geophysical Research*, v.
 561 104, p. 5381-5391.

562 Lintern, D.G., Hill, P.R. and Stacey, C., 2016, Powerful unconfined turbidity current captured
 563 by cabled observatory on the Fraser River delta slope, British Columbia, Canada,
 564 *Sedimentology*, v. 63, p. 1041-1064.

565 Lowe, R.J., Linden, P.F. and Rottman, J.W., 2002, A laboratory study of the velocity structure
 566 in an intrusive gravity current, *Journal of Fluid Mechanics*, v. 456, p. 33-48.

567 Lupi, M. and Miller, S.A., 2014, Short-lived tectonic switch mechanism for long- term pulses
 568 of volcanic activity after mega-thrust earthquakes, *Solid Earth*, v. 5, p. 13-24.

MathWorks^R, 2018, Granulometry of snowflakes. Available online at
[https://uk.mathworks.com/help/images/examples/granulometry-of-](https://uk.mathworks.com/help/images/examples/granulometry-of-snowflakes.html)
[snowflakes.html](https://uk.mathworks.com/help/images/examples/granulometry-of-snowflakes.html)

McCaffrey, W.D., Choux, C.M.A., Baas, J.H. and Haughton, P.D.W., 2003, Spatio-temporal evolution of velocity structure, concentration and grain size stratification within experimental particulate gravity currents, *Marine and Petroleum Geology*, v. 20, p. 851-860.

Mettler-Toledo, 2013, Hardware manual, ParticleTrackTM E25, Inline particle size and count, Mettler-Toledo AutoChem, Inc.

Middleton, G.V. and Hampton, M.A., 1973, Sediment gravity flows: Mechanics of flow and deposition, *Turbidites and Deep Water Sedimentation*, p. 38.

Middleton, G.V., 1993, Sediment deposition from turbidity currents, *Annual Review of Earth Planetary Sciences*, v. 21, p. 89-114.

Mulder, T. and Alexander, J., 2001, The physical character of subaqueous sedimentary density flow and their deposits, *Sedimentology*, v. 48, p. 269-299.

Nortek, 2015, MIDAS Data Acquisition Software: Software User Guide. Boston, MA: Nortek Scientific Acoustic Development Group Inc.

Peakall, J., Felix, M., McCaffrey, W.D. and Kneller, B., 2001, Particulate gravity currents: perspectives, *Special publications of International Association of Sedimentologists*, v. 31, doi:10.1002/9781444304275.ch1.

Piper, D.J.W. and Savoye, B., 1993, Processes of late Quaternary turbidity current flow and deposition on the Var deep-sea fan, north-west Mediterranean sea, *Sedimentology*, v. 40, p. 557-582.

592 Potters, 2018, Spheriglass^R 5000 solid glass microspheres – Technical data sheet, Potters
593 Europe, 3-04-529-1-03.

594 Rimoldi, B., Alexander, J. and Morris, S., 1996, Experimental turbidity currents entering
595 density-stratified water: analogues for turbidites in Mediterranean hypersaline
596 basins, *Sedimentology*, v. 43, p. 527-540.

597 Shanmugam, G., 2002, Ten turbidite myths, *Earth-Science Review*, v. 58, p. 311-341.

598 Sher, D. and Woods, A.W., 2015, Gravity currents: entrainment, stratification and self-
599 similarity, *Journal of Fluid Mechanics*, v. 784, p. 130–162.

600 Simpson, J.E., 1982, Gravity currents in the laboratory, atmosphere, and ocean, *Annual*
601 *Review of Fluid Mechanics*, v. 14, p. 213–234.

602 Simpson, J.E., 1982, Gravity currents in the laboratory, atmosphere, and ocean, *Annual*
603 *Review of Fluid Mechanics*, v. 14, p. 213-234.

604 Stevenson, C.J., Talling, P.J., Wynn, R.B., Masson, D.G., Hunt, J.E., Frenz, M.,
605 Akhmetzhanov, A. and Cronin, B.T., 2013, The flows that left no trace: Very large-
606 volume turbidity currents that bypassed sediment through submarine channels
607 without eroding the sea floor, *Marine and Petroleum Geology*, v. 41, p. 186–205.

608 Stevenson, C. J., Talling, P. J., Masson, D. G., Sumner, E. J., Frenz, M. and Wynn, R. B., 2014,
609 The spatial and temporal distribution of grain-size breaks in turbidites.
610 *Sedimentology* 61(4): 1120-1156.

611 Sultan, N., Gaudin, M., Berne, S., Canals, M., Urgeles, R. and Lafuerza, S., 2007, Analysis of
612 slope failures in submarine canyon heads: An example from the Gulf of Lions, *Journal*
613 *of Geophysical Research: Earth Surface*, v. 112, F01009.

614 Sumner, E. J., Amy, L. A. and Talling, P. J., 2008, Deposit structure and processes of sand
615 deposition from decelerating sediment suspensions. *Journal of Sedimentary*
616 *Research*, v. 78, 529-547.

617 Talling, P.J., Allin, J., Armitage, D.A., Arnott, R.W.C., Cartigny, M.J.B., Clare, M.A., Felletti, F.,
618 Covault, J.A., Girardclos, S., Hansen, E., Hill, P.R., Hiscott, R.N., Hogg, A.J., Clarke, J.H.,
619 Jobe, Z.R., Malgesini, G., Mozzato, A., Naruse, H., Parkinson, S., Peel, F.J., Piper,
620 D.J.W., Pope, E., Postma, M., Rowley, P., Sguazzini, A., Stevenson, C.J., Sumner, E.J.,
621 Sylvester, Z., Watts, C. and Xu, J., 2015, Key Future Directions for Research on
622 Turbidity Currents and Their Deposits, *Journal of Sedimentary Research*, v. 85, p.
623 153–169.

624 Thomas, R.E., Schindfessel, L., McLelland, S.J., Creëlle, S. and De Mulder, T., 2017, Bias in
625 mean velocities and noise in variances and covariances measured using a multistatic
626 acoustic profiler: the Nortek Vectrino Profiler, *Measurement Science and Technology*,
627 v. 28(7), p. 075302.

628 Van Daele, M., Meyer, I., Moernaut, J., De Decker, S., Verschuren, D. and De Batist, M.,
629 2017, A revised classification and terminology for stacked and amalgamated
630 turbidites in environments dominated by (hemi)pelagic sedimentation, *Sedimentary*
631 *Geology*, v. 357, p. 72-82.

632 van de Berg, J.H., Martinius, A.W. and Houthuys, R., 2017, Breaching-related turbidites in
633 fluvial and estuarine channels: Examples from outcrop and core and implications to
634 reservoir models. *Marine and Petroleum Geology*, v. 82, p. 178-205.

635 Wynn, E.J.W., 2003, Relationship between particle-size and chord length distributions in
636 focused beam reflectance measurement: stability of direct inversion and weighting,
637 *Powder Technology*, v. 133, p. 125-133.

Xu, J.P., 2011, Measuring currents in submarine canyons: Technological and scientific progress in the past 30 years, *Geosphere*, v. 7, p. 868-876.

Xu, J.P., Noble, M.A. and Rosenfeld, L.K., 2004, In-situ measurements of velocity structure within turbidity currents, *Geophysical Research Letters*, v. 31, L09311.

Figure captions:

Figure 1 - Experimental set-up. Note: i) aDvp/FBRM data were collected at $x=1.7$ m, 2.7 m and 3.7 m centred at midpoint of offset between the two probes, ii) sediments were sampled at $x=0.7$ m, 1.7 m, 2.7 m, 3.7 m and 4.7 m and iii) the back of the second lockgate (i.e., right end of the flume) starts at 0.15 m position so the absolute distances between sampling positions and source are $x - 0.15$ (m).

Figure 2 - The evolution of single-pulsed flow (0 s delay time).

Figure 3 - The evolution of 2.5 s delay time flow.

Figure 4 - The evolution of 8 s delay time flow.

Figure 5 - aDvp data showing variation in velocity field of A) single-pulsed flows, B) 2.5 s delay time flows and C) 8 s delay time flows. Note that the experimental set-up in which two laterally offset aDvp probes were deployed results in a stitching artefact such that the flows arrived at the upper probe first, then at the lower one 2 s later.

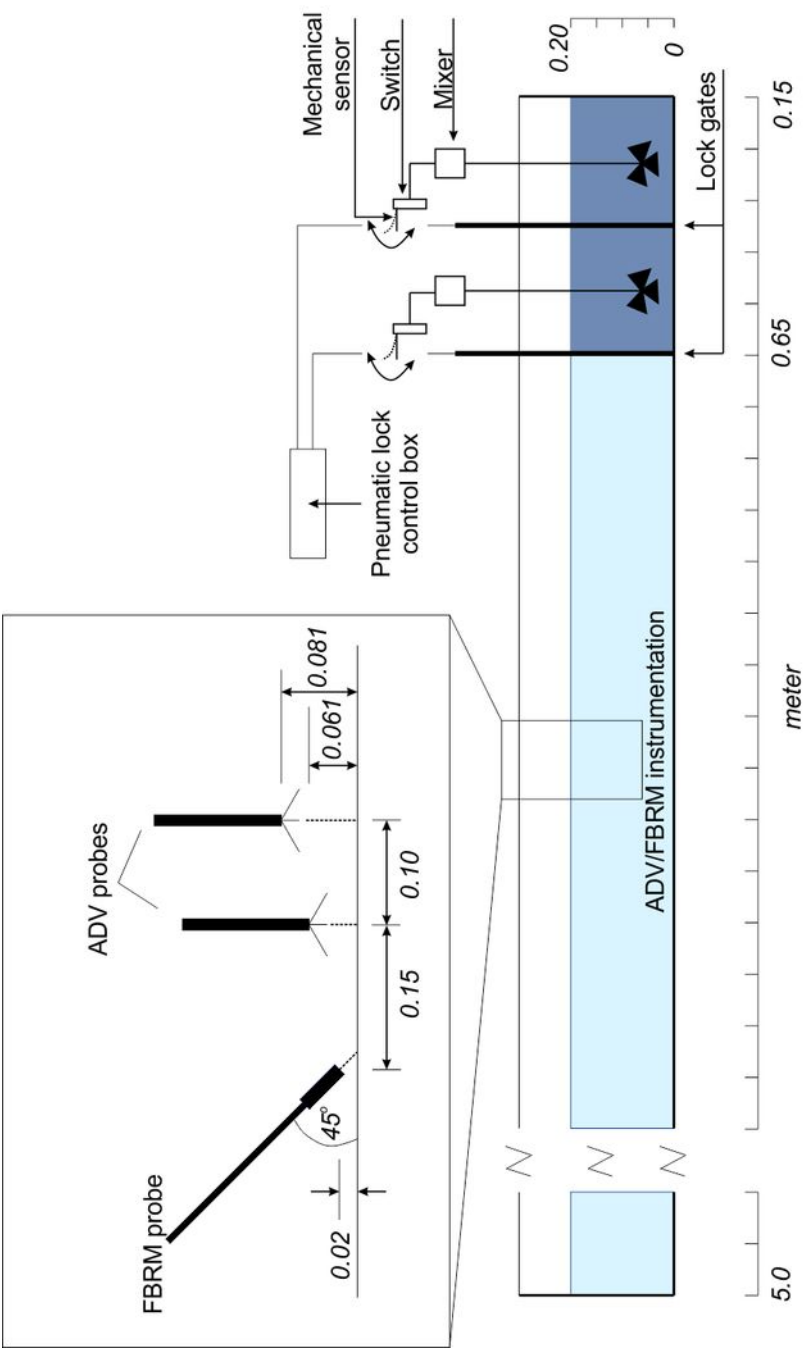
Figure 6 - Depth-averaged velocity of A) 0 s delay time flows, B) 2.5 s delay time flows and C) 8 s delay time flows. Note that effects of surface waves are indicated by the fluctuation of data, especially during waning phases. However, the magnitudes of the waves are relatively small compared to the flow velocity (see e.g., Ho et al. 2018a).

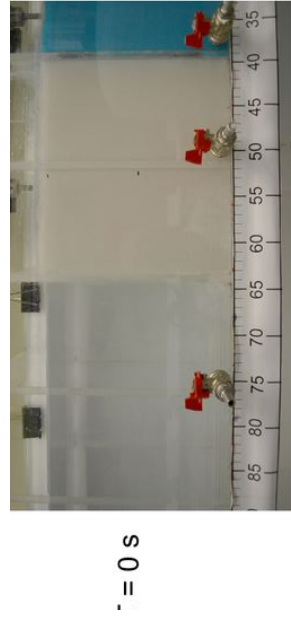
Figure 7 - Real time particle size distribution at 2 cm height of A) single-pulsed flows, B) 2.5 s delay time flows and C) 8 s delay time flows. Note: the reduction in proportions of

662 mean grainsize at 22-25 s, $x=1.85$ m for the 2.5 s delay time flow and that within 34-
663 46 s, $x=1.85$ m for 8 s delay time flow are interpreted as a result of technical glitch.

664 **Figure 8** - Vertical grading profiles of deposits of single-pulsed (2.5 s delay time) and multi-
665 pulsed (8 s delay time) flows collected at 0.7 m, 1.7 m, 2.7 m, 3.7 m and 4.7 m. Notes: i)
666 aDvp data were collected at 1.7, 2.7 and 3.7 m positions (Figs. 5 and 6), ii) Groups A, B and C
667 represent fine, medium and coarse fractions.

668 **Figure 9** - Standard deviation of grain sizes vs depositional thickness.





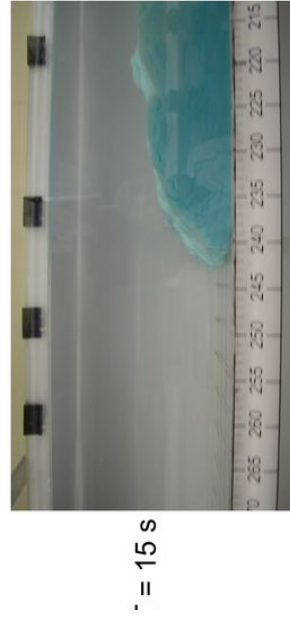
$t = 0 \text{ s}$



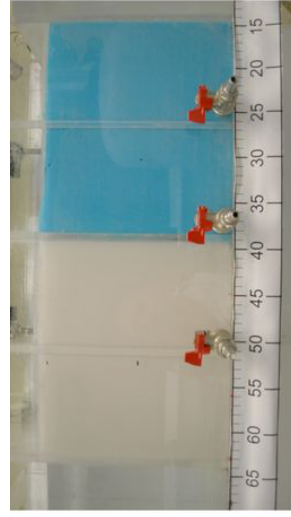
$t = 5 \text{ s}$



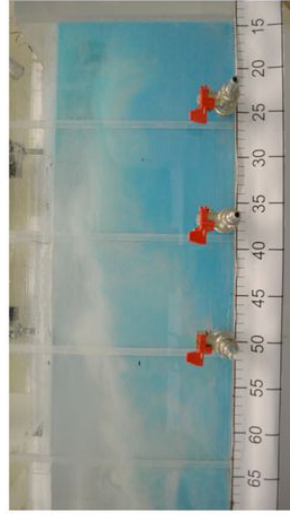
$t = 10 \text{ s}$



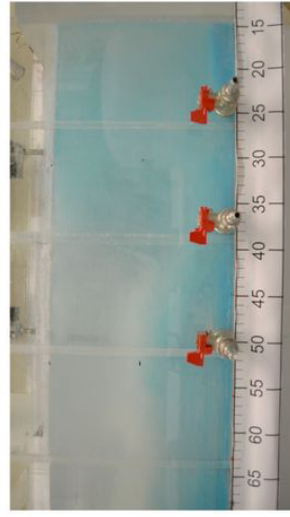
$t = 15 \text{ s}$



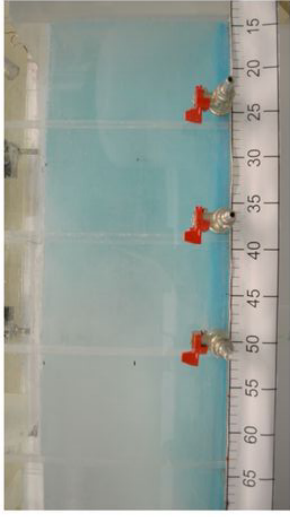
$T = 20 \text{ s}$



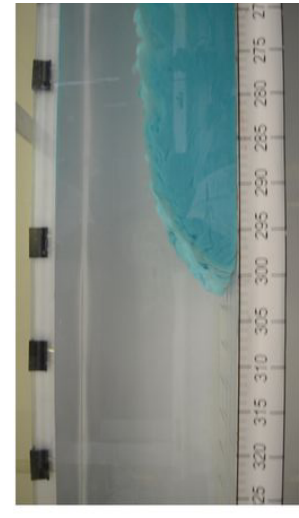
$T = 25 \text{ s}$



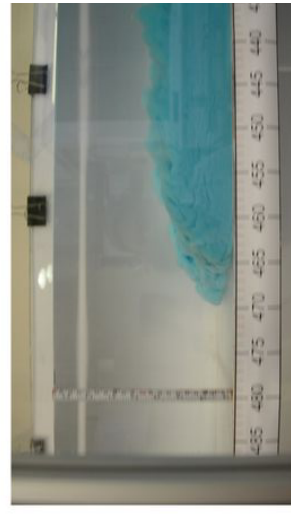
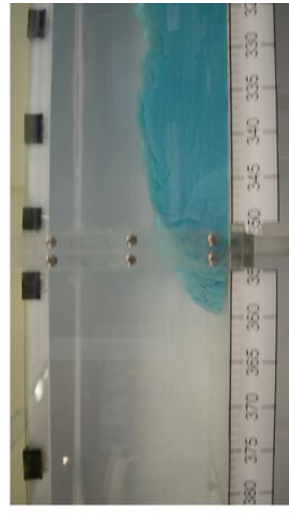
$T = 30 \text{ s}$



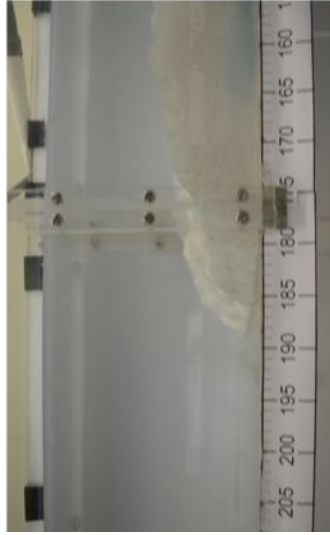
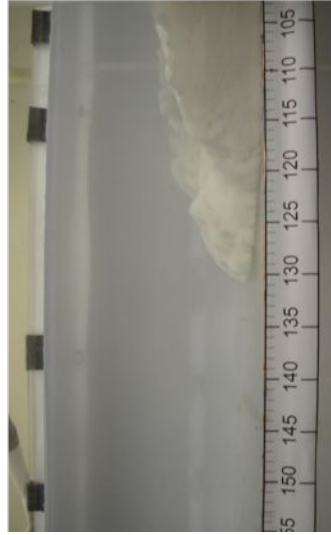
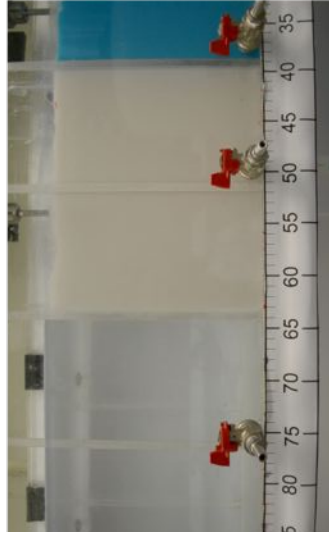
$T = 35 \text{ s}$



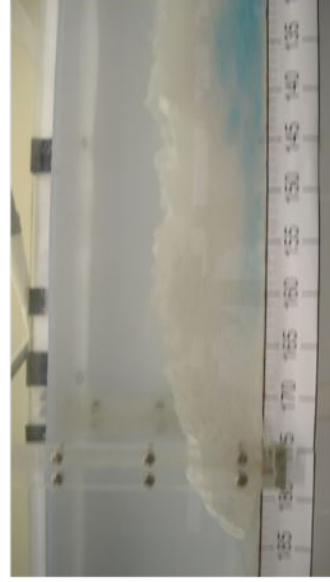
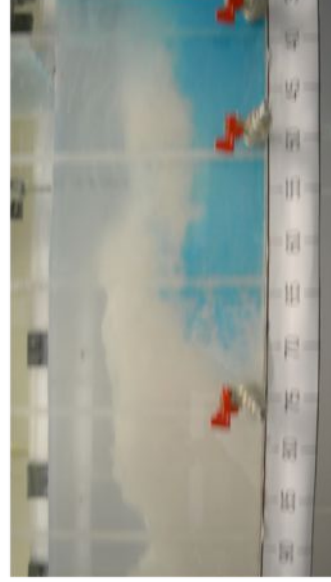
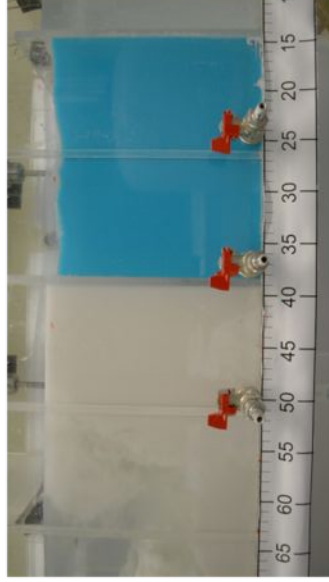
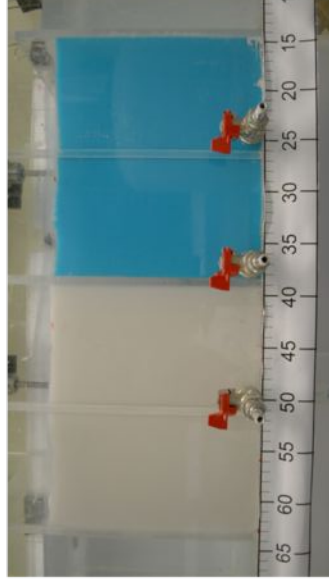
$T = 40 \text{ s}$



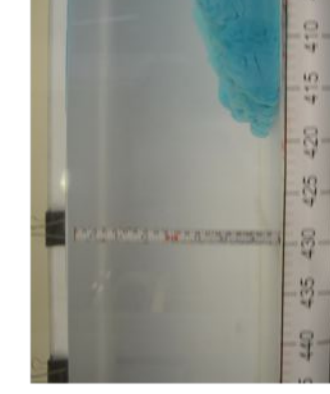
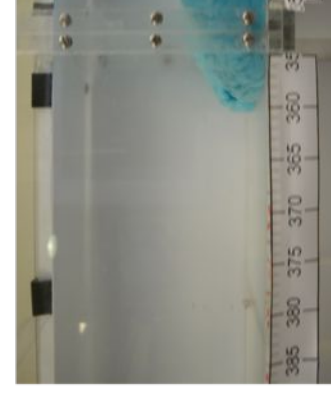
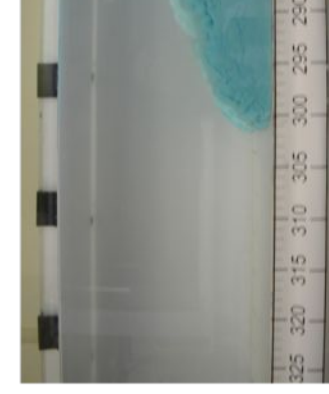
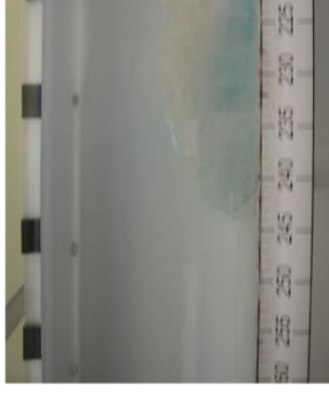
First pulse component



Second pulse component



After point of merg



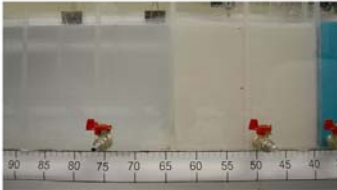
$T = 15 \text{ s}$

$T = 20 \text{ s}$

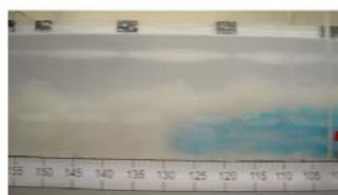
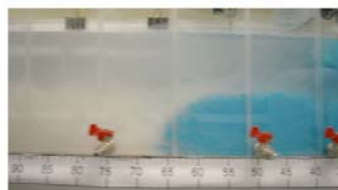
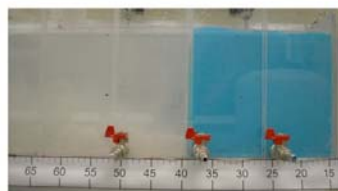
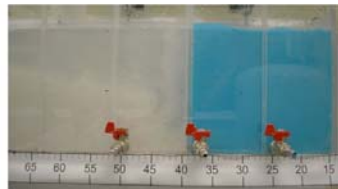
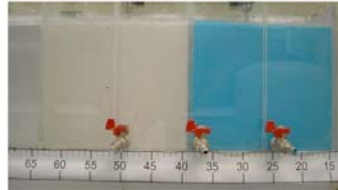
$T = 25 \text{ s}$

$T = 30 \text{ s}$

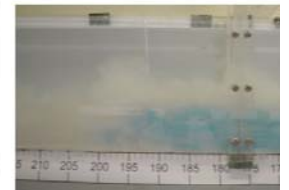
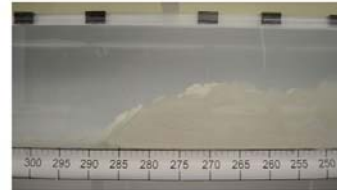
First pulse component



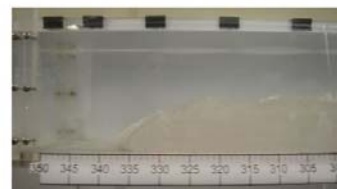
Second pulse component



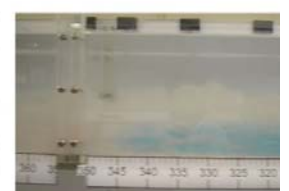
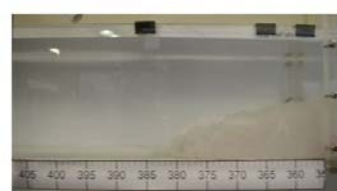
$T = 20 \text{ s}$



$T = 25 \text{ s}$

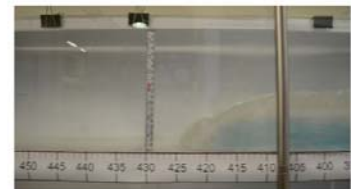


$T = 30 \text{ s}$

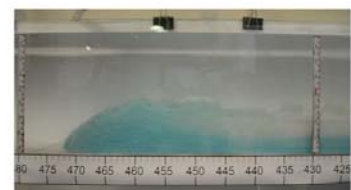


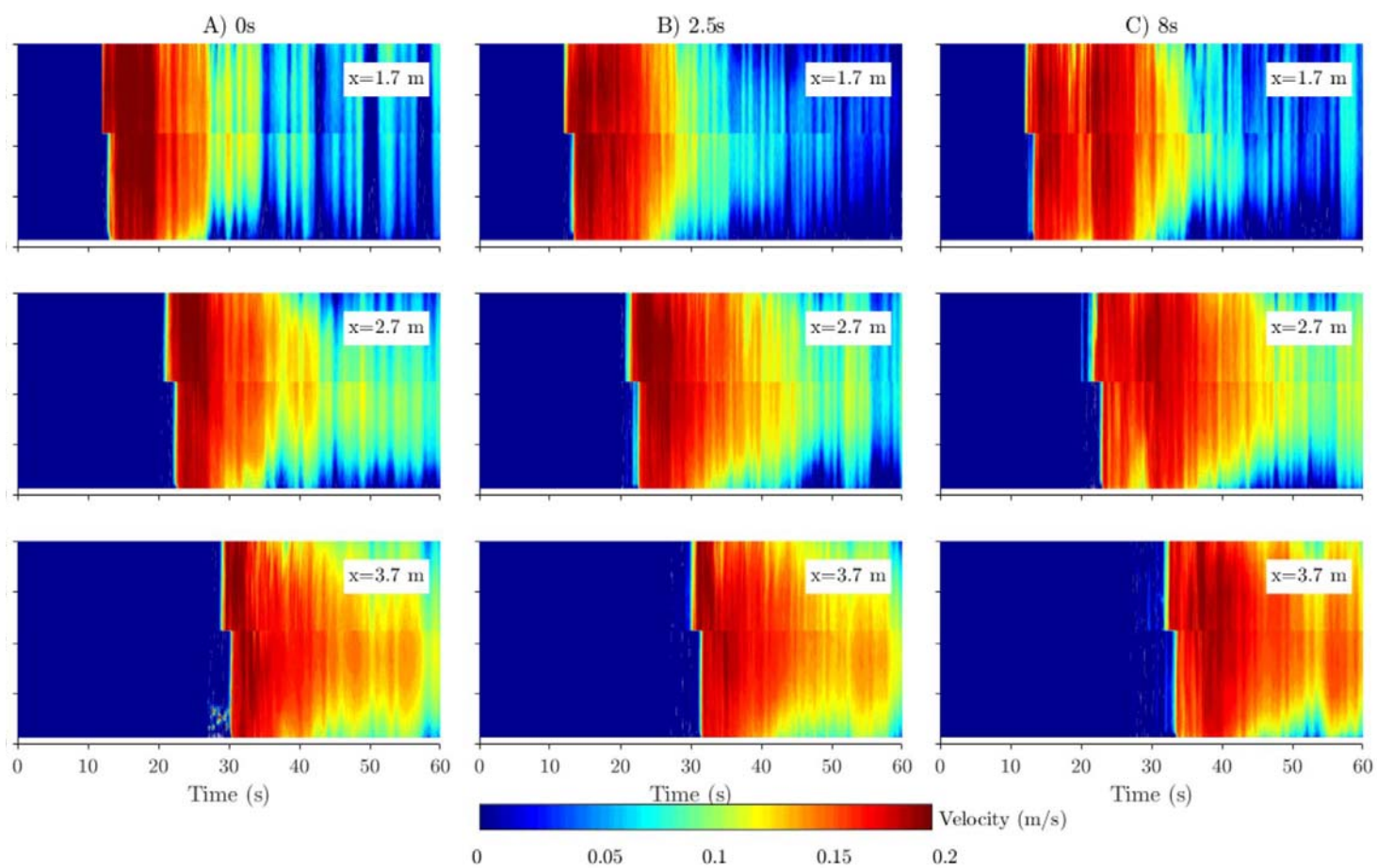
After point of merging

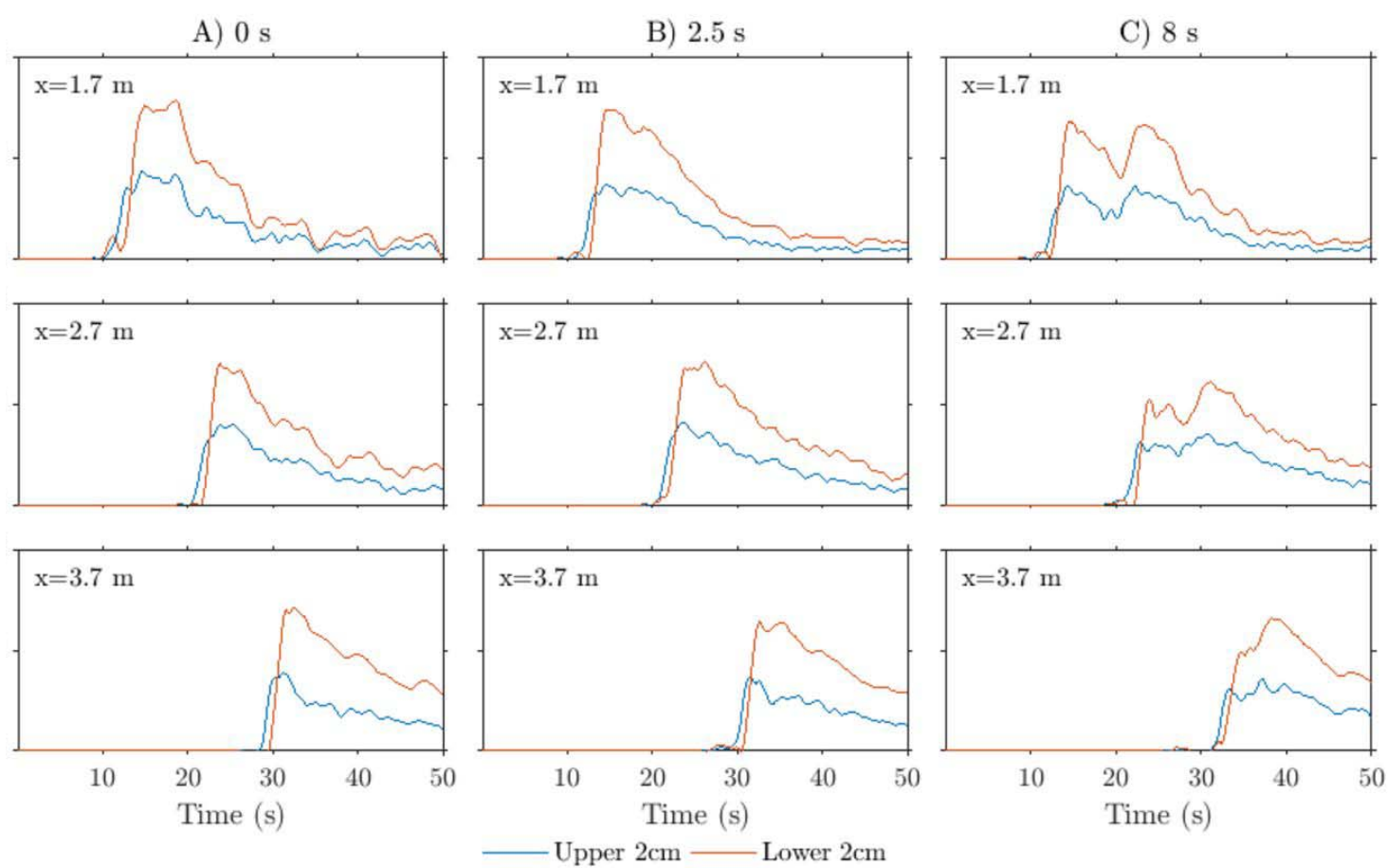
$T = 35 \text{ s}$

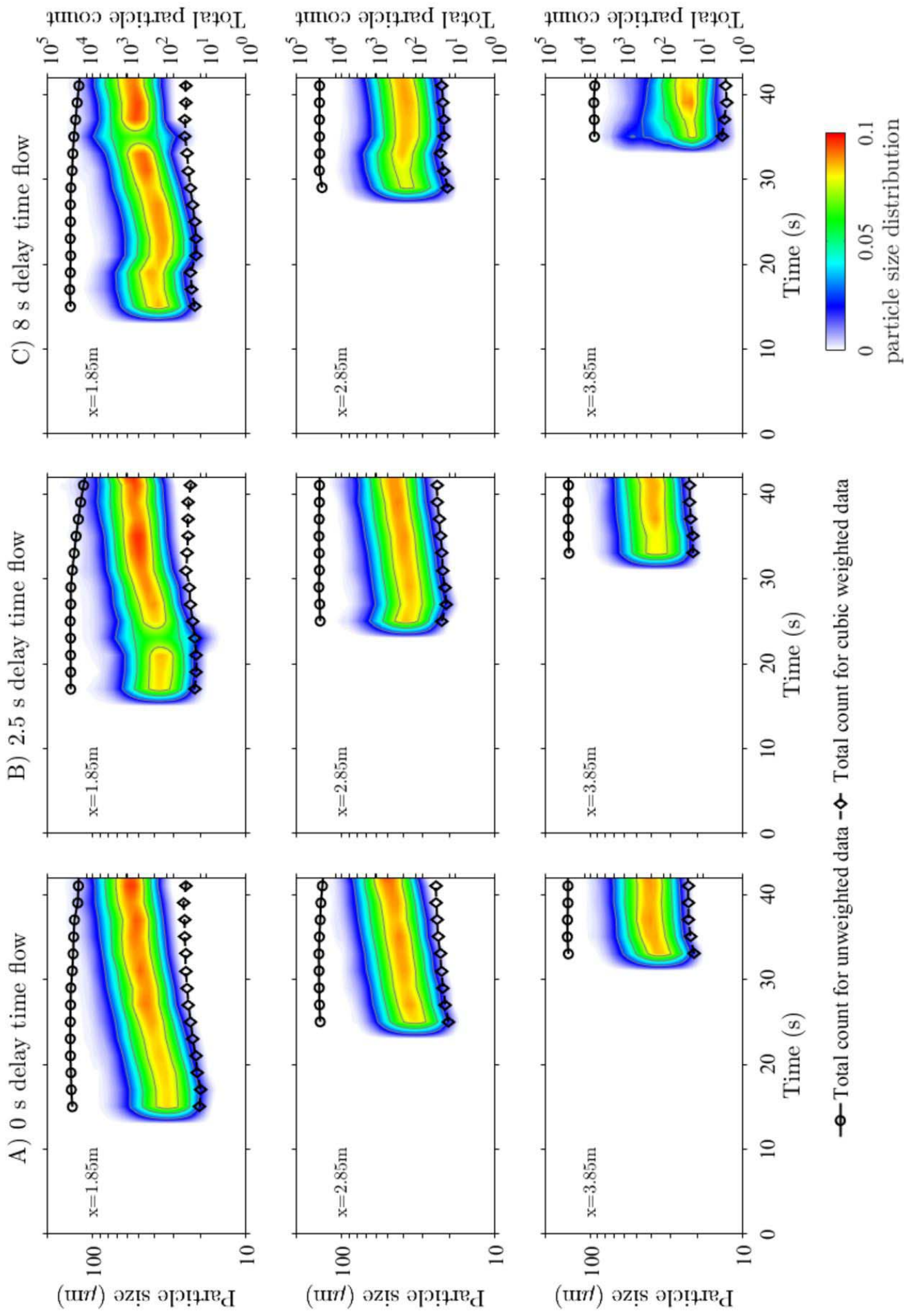


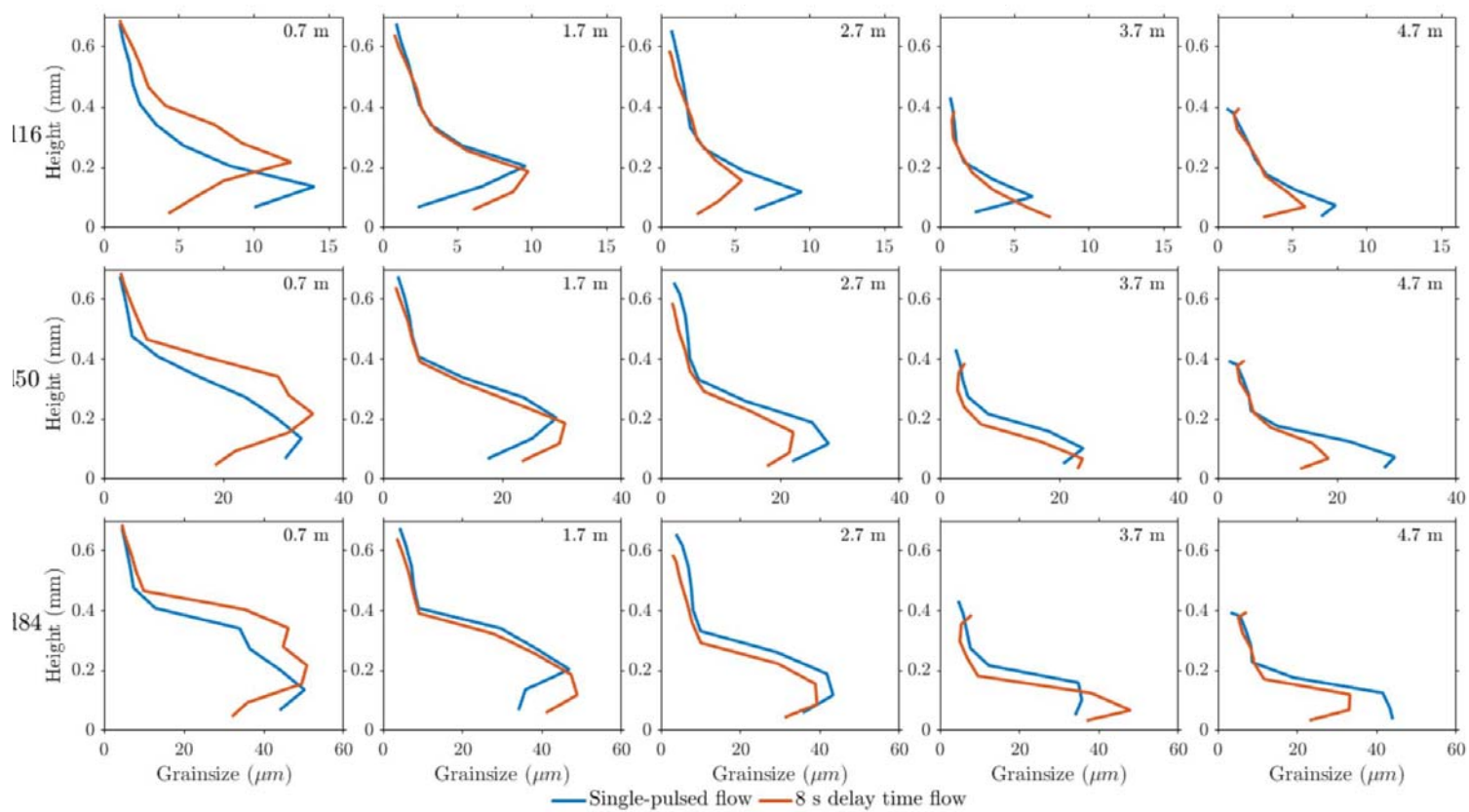
$T = 40 \text{ s}$

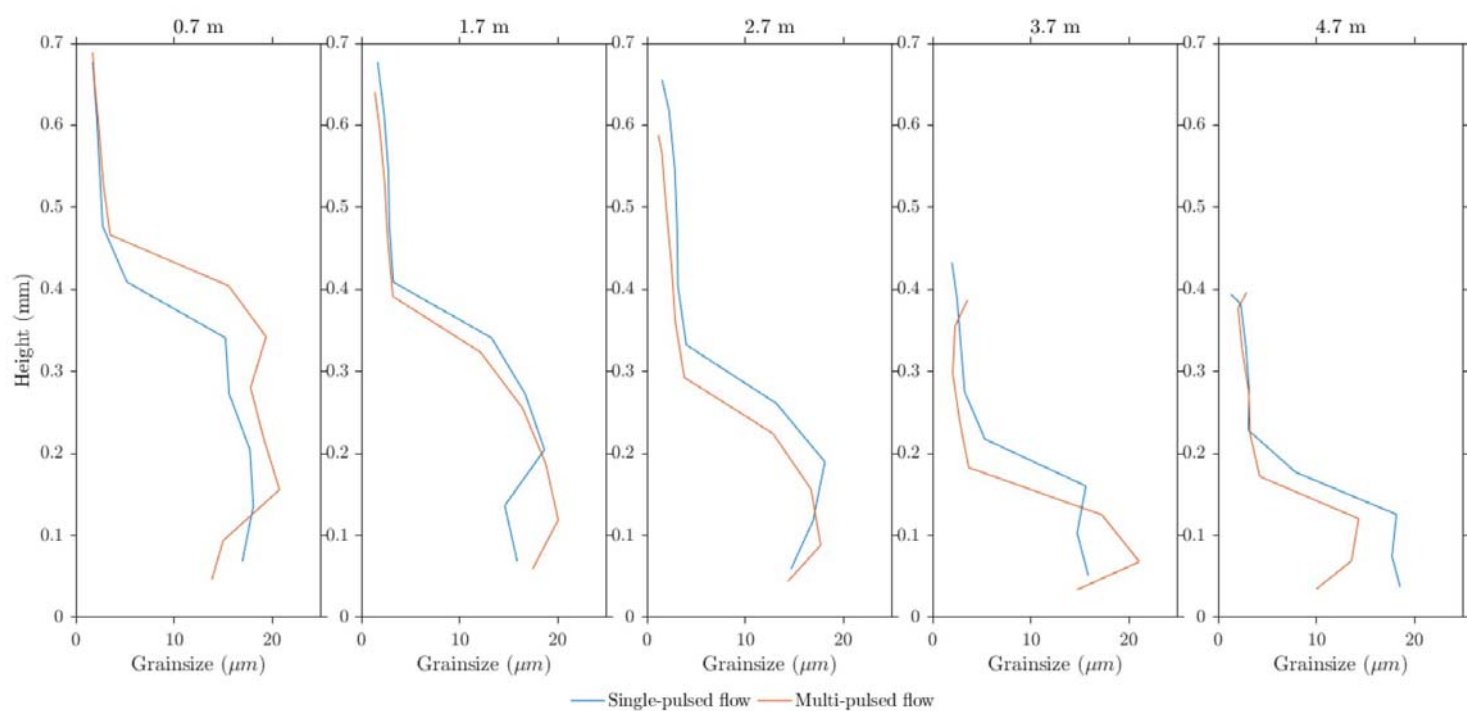












DYNAMICS AND DEPOSITION OF SEDIMENT-BEARING MULTI-PULSED FLOWS AND
GEOLOGICAL IMPLICATION

Viet Luan Ho^{1*}, Robert M. Dorrell², Gareth M. Keevil¹, Robert E. Thomas³, Alan D. Burns⁴,
Jaco H. Baas⁵, William D. McCaffrey^{1†}

¹School of Earth and Environment, University of Leeds, Leeds, UK, LS2 9JT, ²Faculty of
Science and Engineering, University of Hull, Hull, UK, HU6 7RX, ³Energy and Environment
Institute, University of Hull, Hull, UK, HU6 7RX, ⁴School of Process and Chemical Engineering,
University of Leeds, Leeds, UK, LS2 9JT, ⁵School of Ocean Sciences, Bangor University,
Anglesey, UK, LL59 5AB.

* Currently at Imperial College London, London, UK, SW7 2AZ.

Key words: multi-pulsed turbidites, pulsed turbidites, multi-pulsed flows, single-pulsed
turbidites, sediment-bearing flows

Supplementary materials

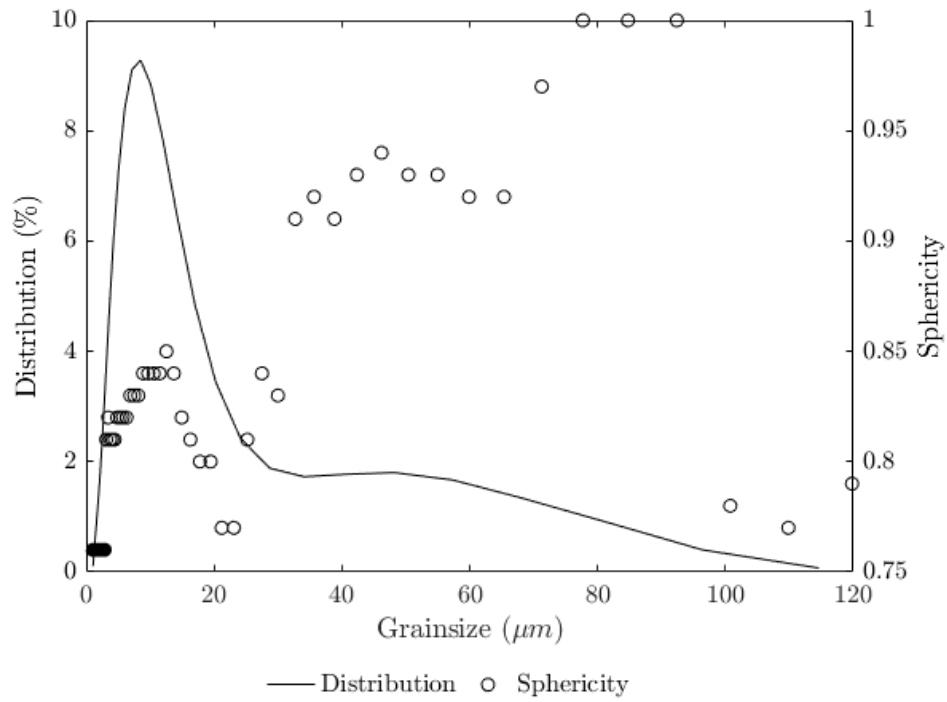


Figure A-1 - Grain size distribution and grain shape data of sediments in the lockboxes used in the experiments.

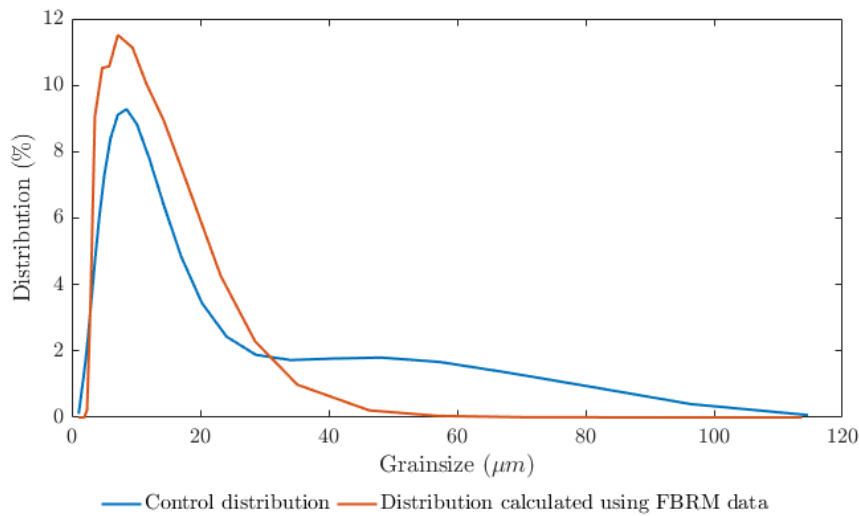


Figure A-2 - Comparison between two data sets of grain size distribution analysed using the same control mixture of sediments; such control mixture is representative of the composition of sediments used in the lockboxes. Note: i) analysis using laser diffraction granulometry method, blue curve (by deploying Malvern 2000e), ii) analysis using FBRM measurement and inversion, red curve and iii) this plot indicates that the reliability of the inversion algorithm is acceptable.